Optical Engineering

SPIEDigitalLibrary.org/oe

Impact of the accurateness of bidirectional reflectance distribution function data on the intensity and luminance distributions of a light-emitting diode mixing chamber as obtained by simulations

Jan Audenaert
Frédéric B. Leloup
Bart Van Giel
Guy Durinck
Geert Deconinck
Peter Hanselaer

SPIE

Impact of the accurateness of bidirectional reflectance distribution function data on the intensity and luminance distributions of a light-emitting diode mixing chamber as obtained by simulations

Jan Audenaert
Frédéric B. Leloup
Bart Van Giel
Guy Durinck
KU Leuven
Light & Lighting Laboratory
Gebroeders de Smetstraat 1
9000 Gent, Belgium
E-mail: jan.audenaert@kahosl.be

Geert Deconinck
KU Leuven
ESAT/ELECTA
Kasteelpark Arenberg 10 bus 2445
3001 Leuven (Heverlee), Belgium

Peter Hanselaer
KU Leuven
Light & Lighting Laboratory
Gebroeders de Smetstraat 1
9000 Gent, Belgium

Abstract. The reliability of ray tracing simulations is strongly dependent on the accuracy of the input data such as the bidirectional reflectance distribution function (BRDF). Software developers offer the possibility to implement BRDF data in different ways, ranging from simple predefined functions to detailed tabulated data. The impact of the accuracy of the implemented reflectance model on ray tracing simulations has been investigated. A light-emitting diode device including a frequently employed diffuse reflector [microcellular polyethylene terephthalate (MCPET)] was constructed. The luminous intensity distribution (LID) and luminance distribution from a specific viewpoint were measured with a near-field goniophotometer. Both distributions were also simulated by use of ray tracing software. Three different reflection models of MCPET were introduced, varying in complexity: a diffuse model, a diffuse/specular model, and a model containing tabulated BRDF data. A good agreement between the measured and simulated LID was found irrespective of the applied model. However, the luminance distributions only corresponded when the most accurate BRDF model was applied. This proves that even for diffuse reflective materials, a simple BRDF model may only be employed for simulations of the LID; for evaluation of luminance distributions, more complex models are needed. [DOI: 10.1117/1.OE.52.9.095101]

Subject terms: bidirectional reflectance distribution function; luminance distribution; optical mixing chamber; ray tracing.

Paper 130672 received May 7, 2013; revised manuscript received Jul. 2, 2013; accepted for publication Jul. 31, 2013; published online Sep. 3, 2013.

1 Introduction

The main characteristics traditionally investigated when developing a luminaire by means of ray tracing software are the luminous intensity distribution (LID), the illuminance distribution on a task surface, and the luminaire efficiency. However, more and more optical engineers acknowledge the need to investigate the luminance distribution of the luminaire during the development stage.[1] Luminance distributions, i.e., luminance maps, are not only a tool to assess subjective criteria such as the aesthetics of the lit luminaire, but also provide objective information to assess criteria such as contrast and the degree of discomfort glare.[2,3] Indeed, discomfort glare, expressed in terms of the unified glare rating,[4] can be calculated from average luminance values, which are found by dividing far-field intensity values by the surface area of the light source. However, for luminaires having a nonuniform luminance distribution, glare evaluation should be based on luminance maps.[5]

Highly reflective diffuse materials are used very frequently in light-emitting diode (LED) luminaires, especially when the output of individual LED packages is to be combined in an optical mixing chamber, such as in the remote phosphor concept.[6] The role of the optical mixing chamber is important as it causes light emitted by an array of LEDs to be homogenized both angularly and spatially before it reaches a remote phosphor plate[7,8] while maintaining high system efficiencies. Such a highly reflective diffuse material that is already being used in commercial illumination systems is the material microcellular polyethylene terephthalate (MCPET). According to the manufacturers' datasheet, the material has a total reflectance of 99% and a diffuse reflectance of 96%.[9]

The bidirectional reflectance distribution function (BRDF) is used to describe the amount of light scattered by a surface as the direction of illumination and/or viewing is changed. In this paper, we investigate the influence of the implemented BRDF model of the MCPET material on simulated luminance distributions of an illumination system that incorporates the highly reflective diffuse material. Three distinct models were implemented. First, a completely diffuse BRDF model was created based on the total reflectance measured with an integrating sphere. Second, a diffuse/specular reflectance model was defined by combining the integrated sphere measurement with specular reflectance measurements obtained from a goniospectrophotometer.[10] Finally, a third model was created as a table containing all experimental BRDF data.

To compare a luminance map generated by a ray tracer to a luminance map measured by a luminance camera, a prototype of a cylindrical optical mixing chamber was constructed out of MCPET. A model of this prototype was created in TracePro®,[11] a commercial ray tracing software package. For each BRDF model, luminance maps of the optical mixing chamber were simulated and compared with a measured luminance image. Similarly, the LID calculated from these ray trace models were compared with the experimental LID obtained with a near-field goniophotometer (RiGO 801, TechnoTeam).[12,13]

2 Experiment Setup

A cylindrical optical mixing chamber with a diameter of 43 mm and height of 21.4 mm was created out of a 1-mm thick sheet of MCPET material. Four circular holes with 5-mm diameter were drilled in the baseplate of the cavity. The same geometry was also modeled in the ray tracer. Next, a remote phosphor LED module (RPLED)[14] was positioned behind the baseplate in order to create four uniform and Lambertian emitting light sources. The edges of the four circular holes in the baseplate were painted black. The prototype is presented in Fig. 1.

The RPLED module was powered with a current of 10 mA. Luminous flux measurements revealed that each circular light source emits 0.96 lm. An RPLED module was chosen as primary light source as it has a uniform exitance and emits Lambertian at each point across the light-emitting surface. This facilitates the modeling of the four distinct light sources in the ray tracer as Lambertian surface sources, each emitting 500,000 rays. Furthermore, this enables the simulation of a luminance map, typically generated by tracing rays from the observer's point of view toward a light source for which a uniform exitance is assumed. A well-defined LID of the light sources allows for the application of importance sampling.[15] A first simulation revealed that with this geometry and light sources, 40% of the emitted light was incident on the inner surfaces of the model and indeed a suitable mixing chamber was constructed.

3 MCPET BRDF Measurement and Modeling

The spectral BRDF $\boldsymbol{q}_{e,\lambda}$ at wavelength λ is defined as the surface radiance of a sample in a particular viewing direction, due to the scattering of radiation incident from a particular direction of irradiation.

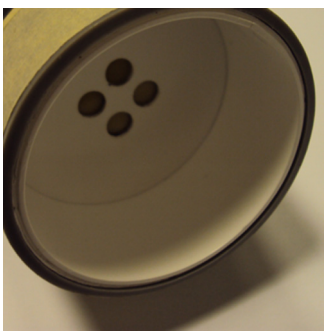

Fig. 1 Prototyped cylindrical mixing chamber constructed out of MCPET including four uniform Lambertian light sources created by partially covering a remote phosphor LED module with an MCPET baseplate.

$$\boldsymbol{q}_{e,\lambda}(\theta_i,\varphi_i,\theta_s,\varphi_s)=\frac{d\boldsymbol{L}_{e,s}(\theta_i,\varphi_i,\theta_s,\varphi_s,\lambda)}{d\boldsymbol{E}_{e,i}(\theta_i,\varphi_i,\lambda)}\left[\frac{1}{sr}\right], \tag{1}$$

with (θ_i, φ_i) being the spherical coordinates of the radiation incident on the surface, (θ_s, φ_s) being the spherical coordinates of the light scattered from the surface, $d\boldsymbol{L}_{e,s}$ being the differential spectral radiance, and $d\boldsymbol{E}_{e,i}$ being the differential spectral irradiance. All spherical coordinates are referenced to the surface normal. To determine the BRDF from goniospectrophotometer measurement data, the American Society for Testing and Materials has proposed the following practical formula:[16]

$$\boldsymbol{q}_{e,\lambda}=\frac{\boldsymbol{\Phi}_{e,\lambda,s}}{\boldsymbol{\Phi}_{e,\lambda,i}\boldsymbol{\Omega}_s|\cos\theta_s|}\left[\frac{1}{sr\cdot nm}\right], \tag{2}$$

with $\boldsymbol{\Phi}_{e,\lambda,s}$ and $\boldsymbol{\Phi}_{e,\lambda,i}$ being the scattered radiant flux toward the detector and the incident radiant flux on the sample, respectively, and $\boldsymbol{\Omega}_s$ being the solid angle of the detector aperture.

In order to perform ray tracing simulations that include the MCPET material, the BRDF of the material has to be modeled in the ray tracer. Three distinct approaches to model the BRDF with increasing complexity were investigated: a completely diffuse model, a diffuse/specular model, and a tabular model. The input data for each model originate from measurements of the reflectance properties of the material.

3.1 *Diffuse BRDF Model*

A completely diffuse model, $BRDF_{diff}$, implies that the BRDF value is constant for every incident direction (θ_i, φ_i) and scatter direction (θ_s, φ_s). The total spectral reflectance, $\boldsymbol{R}_{total}(\lambda)$, of the MCPET material was determined in a sphere-based spectrophotometer (Hunterlab, UltraScan Pro) and is shown in Fig. 2 along with the relative spectrum emitted by the RPLED module.

From Fig. 2, it becomes clear that the variation of the total spectral reflectance over the LED emission wavelength interval can be neglected. This is a tremendous advantage during ray tracing simulations as only one wavelength will need to be traced and/or analyzed. To this end, the total reflectance ($\boldsymbol{R}_{total}$) of MCPET is calculated as a mean value weighted by the relative spectrum of the RPLED module, and equals 98.4% (absorbance of 1.6%). The BRDF value for a completely diffuse material is calculated as

$$\boldsymbol{q}=\frac{\boldsymbol{R}_{total}}{\pi}\left[\frac{1}{sr}\right] \tag{3}$$

and becomes 0.313 sr^{-1}.

3.2 *Diffuse/Specular BRDF Model*

A diffuse/specular BRDF model, $BRDF_{diff/spec}$, requires more measurements but offers a more accurate description of the real BRDF. Spectral specular reflectance measurements were performed using a goniospectrophotometer[10] in which the MCPET sheet is positioned under an incident angle θ_i ranging from near-normal incidence to near-grazing angle. The spectral specular reflectance values, $\boldsymbol{R}_{spec}(\lambda,\theta_i)$, are again weighted with the spectrum of the RPLED module and are called $\boldsymbol{R}_{spec}(\theta_i)$. The values of $\boldsymbol{R}_{spec}$ are plotted and

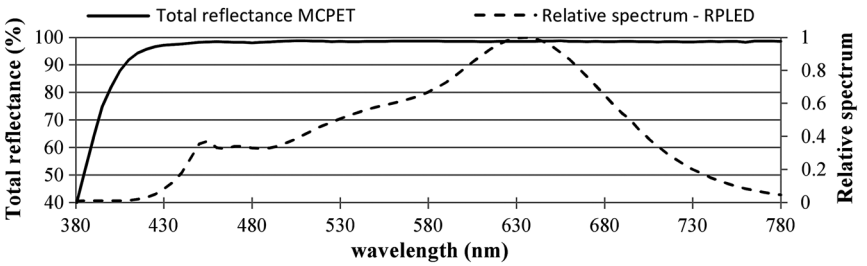

Fig. 2 Total reflectance of MCPET (solid line) and the relative spectrum of the RPLED module (dashed line) across the visual region.

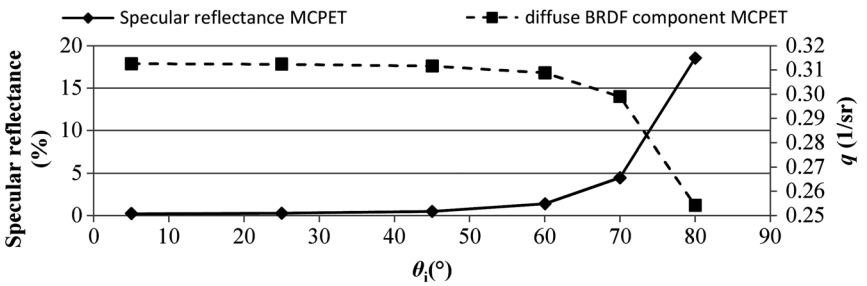

Fig. 3 Specular reflectance values of MCPET (solid line) and diffuse BRDF component (dashed line) for the incident angles of 5, 25, 45, 60, 70, and 80 deg.

displayed for the incident angles of $\theta_i = 5$, 25, 45, 60, 70, and 80 deg in Fig. 3. The values are combined with $\boldsymbol{R}_{\text{total}}$ in order to create a diffuse/specular BRDF model. For each incident angle, a corresponding diffuse BRDF component can be calculated as follows:

$$\boldsymbol{q}_{\text{diff}} = \frac{\boldsymbol{R}_{\text{total}} - \boldsymbol{R}_{\text{spec}}(\theta_i)}{\pi} \left[\frac{1}{\text{sr}}\right]. \tag{4}$$

These diffuse BRDF values remain constant for every scatter direction (θ_s, φ_s), but change with the incident angle θ_i as $\boldsymbol{R}_{\text{spec}}$ also changes with the incident angle. This correlation is also shown in Fig. 3.

3.3 *Tabular BRDF Model*

The final approach, BRDF_{tab}, which is also the most accurate representation of the real BRDF, is formulated in the ray tracer as a lookup table. Scattered flux measurements at scatter angles (θ_s, φ_s), located in the plane of incidence (Π_1) and in a plane Π_2 perpendicular to the plane of incidence and through the specular direction, were performed for the incident angles of $\theta_i = 5$, 25, 45, 60, 70, and 80 deg using the goniospectrophotometer. The corresponding BRDF values are calculated according to Eq. (2) and weighted with the spectrum emitted by the RPLED module. The BRDF measured in the planes Π_1 and Π_2 are shown in Figs. 4(a) and 4(b), respectively. If necessary, the ray tracing software will automatically perform a linear interpolation between the values in the lookup table for any (θ_i, φ_i, θ_s, φ_s) combination not present in the table.

4 Experimental Validation

The geometry of the optical mixing chamber, the characteristics and the position of the four light sources, and the optical properties of the MCPET material were used as input data

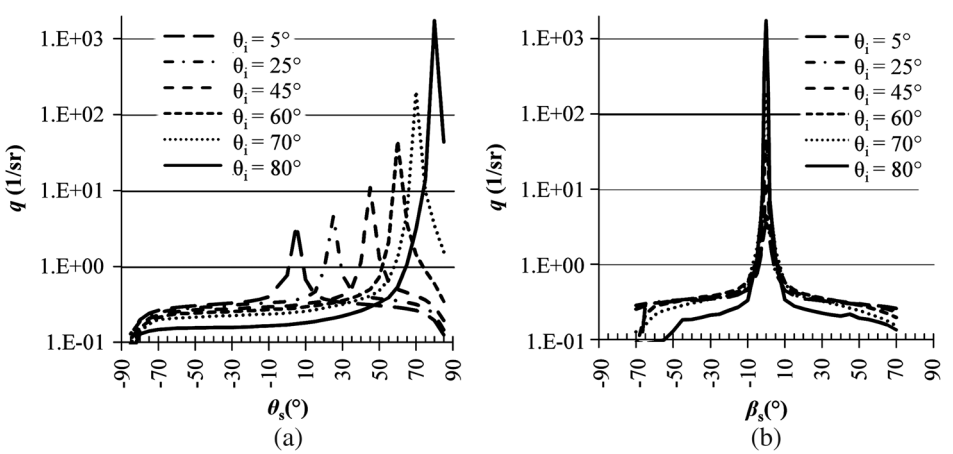

Fig. 4 (a) Measured BRDF of MCPET in the plane of incidence. (b) Measured BRDF of MCPET in a plane perpendicular to the plane of incidence and through the specular direction. θ_s and β_s define the angular offset of each scatter direction to the normal and specular direction, respectively.

in the ray tracing software. A luminance map for an observer positioned at an angle 55 deg away from the direction perpendicular to the baseplate of the mixing chamber was calculated. This angle was chosen specifically, as none of the four separate light sources can be viewed directly. The luminance image is composed of 125×300 pixels of 0.2-mm width located in a plane perpendicular to the viewing direction and through the center of the aperture of the cavity. For each pixel, 1000 rays were traced from the observer point of view toward the optical mixing chamber. Luminance map calculations were performed with each of the three different BRDF models applied to the surfaces of the optical mixing chamber. Furthermore, a high dynamic range luminance image was captured using a luminance camera of a near-field goniophotometer[12] positioned at exactly the same observer position as in the ray tracing software. Figure 5 shows an overview of the simulated luminance images for each BRDF approach [Figs. 5(a) to 5(c)], together with the measured luminance image [Fig. 5(d)].

The experimental luminance image contains four highlights, each originating from one of the circular light sources in the cavity. In Fig. 5(a), however, no highlights can be distinguished. This is to be expected as the surfaces of the cavity are modeled using the completely diffuse $\mathrm{BRDF}_{\mathrm{diff}}$ approach. On the other hand, the simulated luminance image obtained with the $\mathrm{BRDF}_{\mathrm{diff/spec}}$ approach does contain four distinct highlights. Yet, these highlights have very sharp edges, much unlike the blurred highlights found in the measured luminance image. These sharp edges originate from the diffuse/specular modeling approach, as the nondiffuse component in this model is scattered only into one single direction (i.e., the specular direction). When the $\mathrm{BRDF}_{\mathrm{tab}}$ model is applied to the mixing chamber surfaces, as seen in Fig. 5(c), a much better resemblance with the measured luminance image is obtained. Due to a wider angular scattering around the specular reflection direction (cf. Fig. 4), the reflected highlights also become blurred now. A clear difference between the peak luminance value of the highlights is also visible for the $\mathrm{BRDF}_{\mathrm{diff/spec}}$ and $\mathrm{BRDF}_{\mathrm{tab}}$ approach, the latter showing a high resemblance with the peak luminance values of the measured luminance image.

A more quantitative way to compare these luminance images is to calculate the normalized cross-correlation ratio (NCC),[17] a method for template matching, and the normalized root-mean-squared error (NRMSE) between the luminance image and the simulated luminance maps. The NCC and NRMSE are determined by Eqs. (5) and (6), respectively.

$$\mathrm{NCC} = \frac{\sum_{x,y}\{[\boldsymbol{L}_m(x,y) - \bar{\boldsymbol{L}}_m][\boldsymbol{L}_s(x,y) - \bar{\boldsymbol{L}}_s]\}}{\left\{\sum_{x,y}[\boldsymbol{L}_m(x,y) - \bar{\boldsymbol{L}}_m]^2 \sum_{x,y}[\boldsymbol{L}_s(x,y) - \bar{\boldsymbol{L}}_s]^2\right\}^{1/2}}, \tag{5}$$

$$\mathrm{NRMSE} = \frac{\sum_{x,y}\sqrt{\left[\boldsymbol{L}_s(x,y) - \boldsymbol{L}_m(x,y)\right]^2}}{\max(\boldsymbol{L}_s, \boldsymbol{L}_m)}, \tag{6}$$

with $\boldsymbol{L}_m$ and $\boldsymbol{L}_s$ being the measured and simulated luminance values, respectively, while $\bar{\boldsymbol{L}}_m$ and $\bar{\boldsymbol{L}}_s$ denote the mean values of the respective luminance map and x and y the pixel coordinates. The NCC value can range from 0 to 100%, with 0% meaning no correlation at all, while 100% implies that there is a perfect match between the relative shape of the luminance maps. Note that this value only describes a measure of similarity.[18] Therefore, it is essential to calculate both the NCC value and the NRMSE value as the latter takes into account the absolute differences of the luminance maps. For each luminance image, a particular region around the specular highlights was extracted as illustrated in Fig. 6. NCC, NRMSE, maximum, and mean values of these regions were calculated and are displayed in Table 1. Additionally, the uniformity ratio (U) of each region around the specular highlights ranging from $Y = 15$ to 23 mm and $X = 15$ to

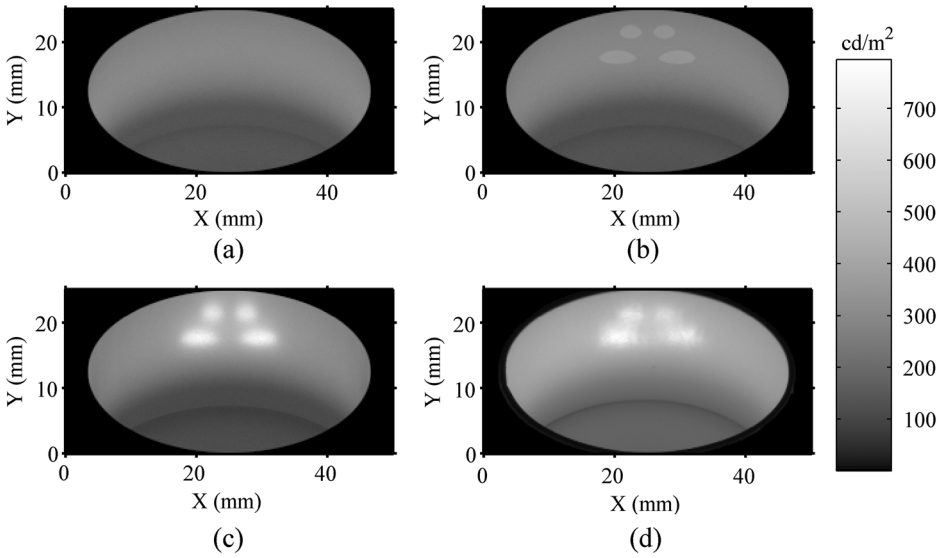

Fig. 5 Gray scale luminance images of the optical mixing chamber with the observer position 55 deg away from the direction perpendicular to the base plate. (a), (b), and (c) are simulated luminance images obtained with $\mathrm{BRDF}_{\mathrm{diff}}$, $\mathrm{BRDF}_{\mathrm{diff/spec}}$, and $\mathrm{BRDF}_{\mathrm{tab}}$ applied to the surfaces of the optical mixing chamber, respectively. (d) Measured luminance image of the prototyped optical mixing chamber.

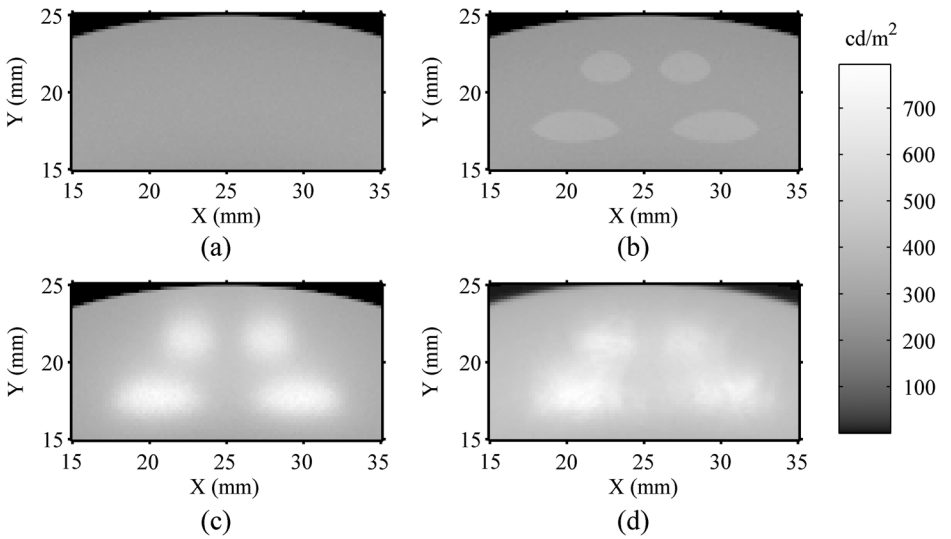

Fig. 6 Extracted region of the gray scale luminance images of the optical mixing chamber that includes specular highlights at an observer position 55 deg away from the direction perpendicular to the baseplate. (a), (b), and (c) are simulated luminance images obtained with $BRDF_{diff}$, $BRDF_{diff/spec}$, and $BRDF_{tab}$, respectively, applied to the surfaces of the optical mixing chamber. (d) Measured luminance image of the prototyped optical mixing chamber.

35 mm is calculated as the ratio of the minimum value to the mean value and is listed in Table 1.

As expected from the visual inspection of the luminance images [Figs. 6(a) to 6(d)], the NCC and NRMSE values, respectively, increase and decrease when the representation of the BRDF of the MCPET material becomes more accurate. The best result is achieved when attributing the most accurate, yet most time-consuming, BRDF model ($BRDF_{tab}$) to the surfaces of the optical mixing chamber. With a value of 95% for NCC and 9% for NRMSE, the simulation results can be classified as very successful. Note that the uniformity ratio of $BRDF_{tab}$ is highly similar to the uniformity ratio of the measured luminance map while this is not the case for the luminance map obtained with the $BRDF_{diff}$ and $BRDF_{diff/spec}$ model. This illustrates the strength of simulation software in predicting luminance maps when accurate input data are available. Deviations from perfect validation might originate from the fact that the prototyped mixing chamber is not an exact replica of the virtual model, as slight deviations of the geometry can occur. Also note that the edges of the circular holes in the baseplate are painted black, whereas in the simulations they are modeled as perfect absorbers.

It might seem strange that even though the scattered luminous flux in the specular direction remains the same for both the $BRDF_{tab}$ and $BRDF_{diff/spec}$ model, an important difference in peak luminance value is observed (Table 1). A possible reason might be found in the fact that the spatially extended light sources are located in proximity of the surfaces of the cavity. Due to this, light emitted from the source

Table 1 Validation of the simulated luminance maps of the virtual model with the three different BRDF models compared to the luminance image of the prototyped optical mixing chamber expressed by means of the calculated NCC and NRMSE values of the region around the specular highlights.

Near-field	NCC (%)	NRMSE (%)	Max (cd/m^2)	Mean (cd/m^2)	U
Measurement	—	—	794	470	0.68
$BRDF_{diff}$	80.07	28.32	309	265	0.87
$BRDF_{diff/spec}$	86.96	27.54	356	268	0.85
$BRDF_{tab}$	94.61	9.14	783	416	0.65

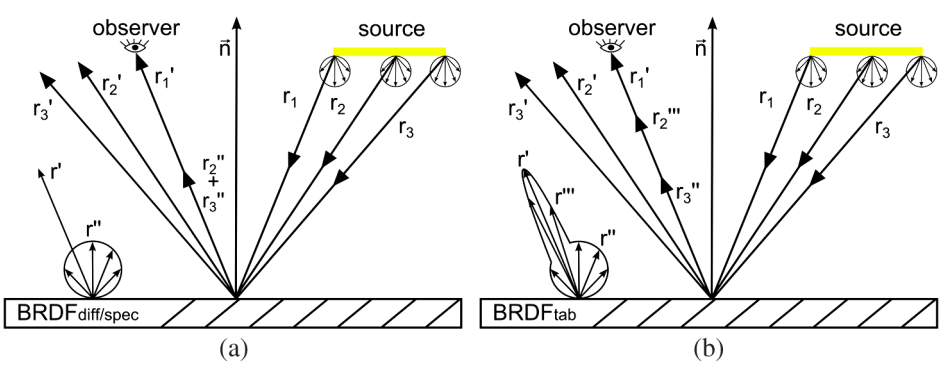

Fig. 7 Schematic representation of the luminance contribution caused by specular (r'), diffuse (r''), and near-specular (r''') reflection with the $BRDF_{diff/spec}$ (a) and $BRDF_{tab}$ (b) model applied to a surface in proximity to a spatially extended light source.

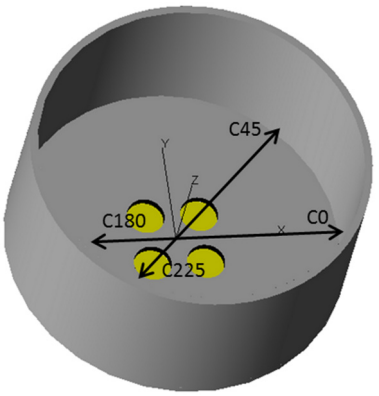

Fig. 8 Virtual model of the optical mixing chamber showing the orientation of the C0-C180 and C45-C225 planes.

going toward a point on the wall of the cavity will hit this point under different incident angles. Furthermore, the $BRDF_{tab}$ model scatters a portion of the incident light toward a wide angular range around the specular component (near-specular reflection), while the $BRDF_{diff/spec}$ model does not contain this contribution. As a result, the highlights obtained with the $BRDF_{diff/spec}$ approach originate almost exclusively from a specular reflection component. However, the highlights obtained with the $BRDF_{tab}$ approach originate from the specular reflection component together with an important near-specular reflection contribution. A schematic of this is presented in Fig. 7.

Simulations of LID were performed with each of the BRDF models applied to the surfaces of the mixing chamber. The LID of the prototyped mixing chamber was also determined with a near-field goniophotometer. Cross-sections of the LID were made at the C0-C180 and C45-C225 planes, which are defined as shown in Fig. 8.

A very good agreement between the simulated and measured LID is achieved as can be seen in Fig. 9, regardless of the BRDF model that is applied to the surfaces of the optical mixing chamber. It seems that the required accuracy level of the BRDF data for predicting far-field intensity distributions is much less stringent than for predicting luminance maps. Indeed, if the specular reflection component is small compared to the total reflectance, far-field calculations are rather insensitive to any particular spatial variations of luminance. Moreover, the intensity within one direction can be considered as a spatial integration of the luminance as viewed from that direction. As a consequence, particular spatial variations will be cancelled out, and the intensity distribution will become similar as long as the same amount of power is emitted into that direction.

5 Conclusion

In this paper, it was investigated to what extent the BRDF of a strongly diffuse reflective material should be measured and/or modeled in order to accurately simulate far-field intensity distributions and near-field luminance distributions. The study is based on ray tracing simulations of an optical mixing chamber obtained with a commercially available reflective material. Three BRDF approaches to model this material, characterized by increasing complexity, amount of required input data, and measuring time, have been considered.

Comparison between the simulated and the experimental LID showed a high correlation regardless of the BRDF model being applied to the surfaces of the optical mixing chamber. Indeed, the grade of detail of the description of the specular reflection component of such a strongly diffuse reflective material does not have a large impact on far-field calculations. However, although the material is highly diffuse, the modeling accuracy and elaboration of the specular reflection component, which becomes more prominent for larger angles of incidence, do have an important impact on and determines the predictive power of the simulated luminance maps. Although these results were obtained for one particular mixing chamber, the results highlight the importance to accurately model the BRDF even for highly diffuse materials. For materials exhibiting a stronger specular reflectance component, the difference between luminance maps simulated with various reflectance models will be even much higher.

Keeping these observations in mind, a reduction of the required input data and accordingly the amount of required measurements can be achieved if we know in advance which quantity has to be simulated during simulations of optical systems that incorporate diffuse highly reflective materials. If only the LID is of interest, then relatively few measurements are necessary to construct a simple BRDF model that is adequate enough to predict LIDs accurately. On the other hand, more elaborate BRDF measurements and modeling are essential if a high accuracy of the near-field (luminance

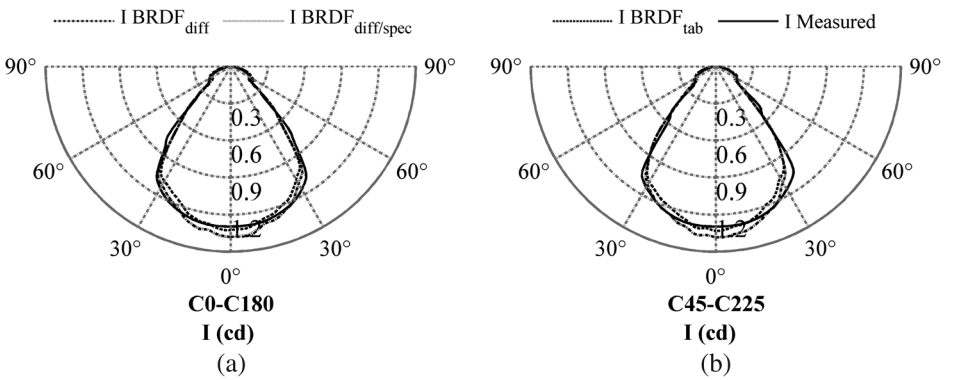

Fig. 9 Validation of the LID of the virtual model when applying the three different BRDF models and as measured (full line). (a) C0-C180 plane. (b) C45-C225 plane.

images in particular) is required. This is especially important when quantities such as uniformity, contrast, and discomfort glare are to be derived from simulated luminance maps.

Acknowledgments

Jan Audenaert thanks the Agency for Innovation by Science and Technology in Flanders (IWT) for financial support (SB-091442). The authors wish to thank the Hercules Foundation for funding the near-field goniophotometers as medium-scale infrastructure project (AKUL-35).

References

1. R. J. Koshel, "Lit appearance modeling of illumination systems," *Proc. SPIE* **4768**, 65–73 (2002).
2. W. Kim, H. T. Ahn, and J. T. Kim, "A first approach to discomfort glare in the presence of non-uniform luminance," *Build. Environ.* **43**(11), 1953–1960 (2008).
3. K. Teppei et al., "Discomfort glare caused by white LED light sources," *J. Light Visual Environ.* **30**(2), 95–103 (2006).
4. International Commission on Illumination., "Discomfort glare in interior lighting," Vol. 117, CIE Publication (1995).
5. Y. Nakamura, "Method of discomfort glare estimation applicable to a wide range of source sizes—glare estimation system based on luminance image," *Light Eng.* **16**(1), 84–88 (2008).
6. C. Hoelen et al., "Remote phosphor LED modules for general illumination—towards 200 lm/W general lighting LED light sources," *Proc. SPIE* **7058**, 70580M (2008).
7. N. Narendran et al., "Extracting phosphor-scattered photons to improve white LED efficiency," *Phys. Stat. Sol. A* **202**(6), R60–R62 (2005).
8. N. Narendran, "Improved performance white LED," *Proc. SPIE* **5941**, 45–50 (2005).
9. American Furukawa Inc., "MCPET datasheet," 2008, http://www.furukawaamerica.com/mcpet.html (27 February 2013).
10. F.B. Leloup et al., "Design of an instrument for measuring the spectral bidirectional scatter distribution function," *Appl. Opt.* **47**(29), 5454–5467 (2008).
11. Lambda Research Corporation, "TracePro®," 2013, http://lambdares.com/ (27 February 2013).
12. K. Bredemeier, R. Poschmann, and F. Schmidt, "Development of luminous objects with measured ray data," *Laser+Photonik* **2**, 20–24 (2007).
13. CIE TC-2-62, "Imaging-photometer-based near-field goniophotometer," CIE Draft No1 (2010).
14. XSM 80 Series LED Module Datasheet, Xicato XSM, 2013, http://www.xicato.com (27 February 2013).
15. P. Dutré, K. Bala, and P. Bekaert, *Advanced Global Illumination*, A K Peters, Ltd., Wellesley, Massachusetts (2006).
16. ASTM., "Standard practice for goniometric optical scatter measurements," ASTM E2387 (2005).
17. J. P. Lewis, "Fast template matching," in *Vision interface*, pp. 120–123, Canadian Image Processing and Pattern Recognition Society, Quebec City, Canada (1995).
18. V. Di Gesù and V. Starovoitov, "Distance-based functions for image comparison," *Pattern Recogn. Lett.* **20**(2), 207–214 (1999).

Jan Audenaert graduated as a master in information and communication technology and started a PhD research project funded by the Agency for Innovation by Science and Technology in Flanders (IWT) at the Light and Lighting Laboratory (Gent, Belgium). His research focuses on ray tracing for non-imaging optics.

Frédéric B. Leloup graduated as a master in industrial engineering from Katholieke Hogeschool (KAHO) Sint-Lieven (Gent) in 2001 and obtained his PhD in engineering from Katholieke Universiteit (KU) Leuven in 2012. He is currently a research support co-ordinator at the Light & Lighting research group, affiliated to the same institution. His research focuses on the soft metrology of appearance, investigating possible correlations between optical parameters which, either singly or in combination, correspond to attributes of visual appearance (color, gloss, texture, etc.). He primarily focuses on gloss measurement and perception.

Bart Van Giel graduated in physics from Gent University in 2004. He has been involved in R&D projects for projection and lighting applications. Currently he is responsible for the technological consultancy in the Light and Lighting laboratory.

Guy Durinck graduated as a master of science in physics from Universiteit Gent in 1989 and obtained a PhD in physics from Katholieke Universiteit Leuven in 1999. He is a lecturer at Katholieke Hogeschool Sint-Lieven and Hogeschool Universiteit Brussel. He teaches mathematics and physics to engineering students and physical optics to students in optometry. His current research interests are in the design of lighting and illumination optics and in optical modeling by ray tracing. He is a member of SPIE.

Geert Deconinck is a full professor at KU Leuven-Department of Electrical Engineering and has a PhD degree in applied science. His research interest focuses on control and information technology for power systems. Examples include smart grids, lighting technology or distributed control of distributed energy resources. He teaches topics related to industrial automation, smart distribution systems, lighting and measurement techniques. He heads the research group Electrical Energy and Computing Architectures (ESAT/ELECTA) and is a fellow of Institute of Engineering and Technology (IET) and a senior member of IEEE.

Peter Hanselaer received his PhD in physics from the University of Gent in 1986. He is an associate professor at the University of Leuven. In 1997, he founded the Light & Lighting Laboratory specializing in spectral optical measurements. His main research areas are lighting, color and appearance, optical design, new light sources, and photovoltaic energy. He is the Belgian delegate in the International commission on Illumination (CIE), division 1. He is teaches physical topics of the master courses lighting and opto-electronics.